**Geomechanics and Engineering**, *Vol. 12*, *No. 4* (*2017*) *579-593*
DOI: https://doi.org/10.12989/gae.2017.12.4.579


# A large-scale test of reinforced soil railway embankment with soilbag facing under dynamic loading

Huabei Liu [1a], Guangqing Yang [*2], He Wang [2b] and Baolin Xiong [2c]

[1] *Huazhong University of Science and Technology*, *Wuhan*, *Hubei 430074*, *China*
[2] *School of Civil Engineering*, *Shijiazhuang Tiedao University*, *Shijiazhuang*, *Hebei 050043*, *China*

(*Received August 25*, *2015*, *Revised April 28*, *2016*, *Accepted November 27*, *2016*)

**Abstract.** Geosynthetic reinforced soil retaining walls can be employed as railway embankments to carry large static and dynamic train loads, but very few studies can be found in the literature that investigate their dynamic behavior under simulated wheel loading. A large-scale dynamic test on a reinforced soil railway embankment was therefore carried out. The model embankment was 1.65 meter high and designed to have a soilbag facing. It was reinforced with HDPE geogrid layers at a vertical spacing of 0.3 m and a length of 2 m. The dynamic test consisted of 1.2 million cycles of harmonic dynamic loading with three different load levels and four different exciting frequencies. Before the dynamic loading test, a static test was also carried out to understand the general behavior of the embankment behavior. The study indicated the importance of loading frequency on the dynamic response of reinforced soil railway embankment. It also showed that toe resistance played a significant role in the dynamic behavior of the embankment. Some limitations of the test were also discussed.

**Keywords:** geosynthetics; reinforced soil embankment; railway; soilbag; large-scale dynamic test

## 1. Introduction

Geosynthetic reinforced soil (GRS) retaining walls can be employed as embankments, bridge abutments, or bridge piers in highways or railways, among which, the applications of geosynthetic reinforced soil in the embankments of railways have been mostly successful in recent decades (Wayne and Miller 1996, Tatsuoka *et al*. 1997, Yang *et al*. 2009a, 2010, Koseki 2012, Lostumbo *et al*. 2014). In these applications, the reinforced soil embankments are subjected to not only the static load from the railway structure, but also the dynamic load from the passing trains. The magnitude and frequency of the dynamic load depend on the characteristics of the passing train and the railway structure (Bian *et al*. 2014). It is necessary to understand the dynamic behavior of the reinforced soil embankment, so that a rational method of analysis and design can be established.

The behavior of reinforced soil retaining walls under static surcharge or footing load has been the subject of a number of studies (Arab *et al*. 2001, Abu-Hejleh *et al*. 2002, Hatami and Bathurst

*Corresponding author, Professor, E-mail: gtsyang@163.com
[a] Professor
[b] Ph.D. Student
[c] Associate Professor


http://www.techno-press.org/?journal=gae&subpage=7 ISSN: 2005-307X (Print), 2092-6219 (Online)

2006, Wu *et al*. 2006, 2013, Adams *et al*. 2011, Liu 2015, Xie and Leshchinsky 2015), which revealed the deformation property, the reinforcing mechanism, the bearing capacity, and some important parameters that influence the reinforced soil response. On a related subject, many studies can be found on the seismic behavior of geosynthetic reinforced soil retaining walls using experimental or numerical approaches (Cai and Bathurst 1996, El-Emam and Bathurst 2007, Liu 2009, Zarnani *et al*. 2011, Bhattacharjee and Krishna 2012, Lee and Chang 2012, Ling *et al*. 2012, Liu and Ling 2012, Liu *et al*. 2011, 2014a, Srilatha *et al*. 2013, Abbasi *et al*. 2014, Guler and Selek 2014, Komak Panah *et al*. 2015, Wang *et al*. 2015). However, the dynamic responses of reinforced soil retaining walls and slopes under surface dynamic loading have seldom been investigated (Uchimura *et al*. 2003, Uchimura and Mizuhashi 2005, Payeur *et al*. 2015). Uchimura *et al*. (2003) investigated the behavior of a prestressed reinforced soil bridge pier under low-frequency cyclic loading, while in Uchimura and Mizuhashi (2005), the importance of reinforcement stiffness on the cyclic response of geosynthetic reinforced soil was discussed. The experimental and numerical study by Payeur *et al*. (2015) showed that a steel Mechanically Stabilized Earth (MSE) wall supporting railway tracks exhibited significant freqency-dependent responses under simulated wheel loading.

As a component in a continuous investigation for the dynamic behavior of GRS railway embankment, a large-scale test was carried out. The model embankment was 1.65 m high, was reinforced with close-spaced HDPE geogrids, and had a soilbag facing. Soilbags have extensive applications in geotechnical engineering (Tatsuoka 1993, Matsuoka and Liu 2003, Lohani *et al*. 2006, Matsushima *et al*. 2008, Nakagawa *et al*. 2008, Huang *et al*. 2008, Xu *et al*. 2008, Yang *et al*. 2010, Ansari *et al*. 2011, Ye *et al*. 2011, Koseki 2012, Kachi *et al*. 2013, Fukubayashi and Kimura 2014, Liu *et al*. 2014a, 2015), one of which is to act as temporary or permanent facings of reinforced soil retaining walls (Tatsuoka 1993, Yang *et al*. 2010, Koseki 2012). The model embankment was subjected to 1.2 million cycles of harmonic dynamic loading with different exciting frequencies.

The large-scale test was designed to reveal the responses and mechanisms of GRS embankments with flexible facing elements subjected to a large number of dynamic loading cycles. The objective is to provide some basis for the application of GRS railway embankments. In addition, the test will serve as an experimental model with simple boundary condition for the calibration of numerical procedures, which may then be employed to investigate the responses and mechanisms of GRS railway embankments with more authentic railway loading and boundary conditions.

## 2. Test setup and procedure

Fig. 1 shows the test setup. The reinforced soil embankment was 1.65 m high. Soilbags were used as its facing elements, the batter angle of which was 16.7°. The test was carried out inside a test box that had a dimension of 3.5 m (Length) by 2.0 m (Height) by 1.0 m (Width), as shown in Fig. 1(a). One side of the test box was transparent so that possible large soil deformation can be observed.

The embankment was backfilled by a poorly-graded gravelly soil (GP as per USCS), the properties of which are shown in Table 1. Each soil layer was compacted by a vibrating tamper for 6 times, resulting in a compacted thickness of 15 cm. The dry unit weight of the compacted soil was monitored during construction using the water replacement method in a test pit (ASTM

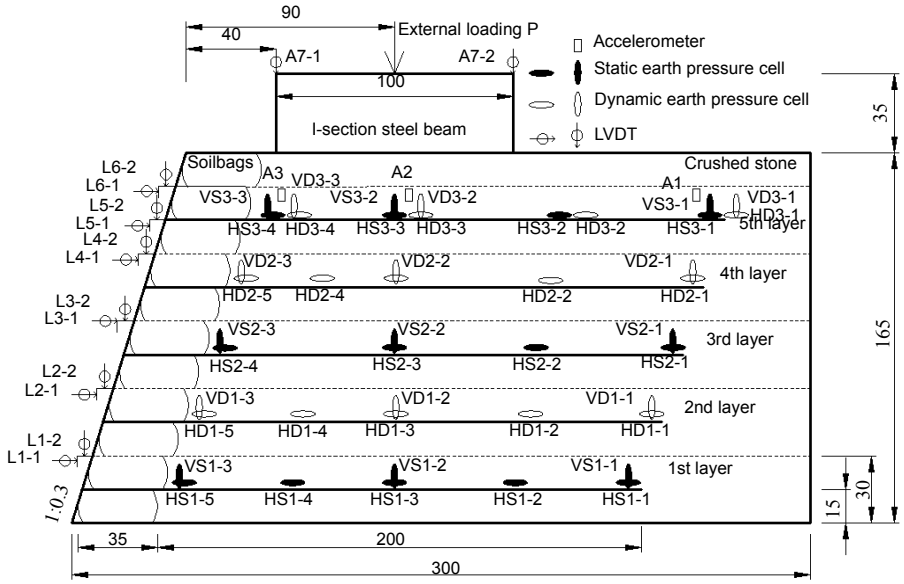


(a)

(b)

Fig. 1 Test setup & completed embankment: (a) Test setup; (b) photo of the completed embankment before loading

Table 1 Properties of the gravelly soil

| Optimal water content | Maxium dry unit weight (kN/m$^3$) | Coefficient of uniformity $C_u$ | Coefficient of gradation $C_c$ | $d_{50}$ (mm) | Relative compaction | Friction angle | Cohesion $c$ (kPa) |
|---|---|---|---|---|---|---|---|
| 8.70% | 22.66 | 17.48 | 0.54 | 4.5 | 92% | 38 | 5 |

D5030-04 2004), and the overall relative compaction was larger than 92%. Large-scale direct shear tests were carried out to determine the soil strength, as shown in Table 1. The size of the

Table 2 Properties of the geogrids

| Material | Type | Rib width (mm) | Rib thickness (mm) | Tensile strength (kN/m) | Strength at 2% strain (kN/m) | Peak strain |
|---|---|---|---|---|---|---|
| HDPE | Uniaxial | 5.3 | 1 | 70 | 18 | 11.80% |

shear box was 30 cm by 30 cm. However, a 15-cm layer of densely compacted crushed stone was used on top of the embankment following common practice in railway engineering (TB 10621 2009, Yang *et al*. 2009b, Bian *et al*. 2014, Payeur *et al*. 2015), so that the simulated wheel load can be better distributed to the embankment soil.

The embankment was reinforced by 5 layers of uniaxial HDPE geogrids at a length of 2 m, the mechanical properties of which are shown in Table 2. The geogrids had a secant stiffness of 900 kN/m at 2% strain. The vertical spacing between the reinforcement layers was 30 cm. The geogrids werer wrapped around the soilbag facing, as shown in Fig. 2(a). In addition, to stretch the geogrids during soil placement and to improve the stiffness of the reinforced soil under vertical loading, the ends of the geogrid layers were anchored to the soil by U-shaped steel pins, as shown in Fig. 2(b). The soilbags were made of polypropylene (PP), and had a dimension of 50 cm by 35 cm by 15 cm after filling. They are filled with the same material as the backfill soil. The soil in the soilbags was compacted during filling, and the overall relative compaction was similar to that of the backfill soil. However, since since accurate volume of a soilbag was difficult to estimate, the actual density might vary for different bags. During construction, the soilbags were also compacted for better alignment.

The simulated wheel load was applied to the layer of crushed stone through a T-section steel beam, the width of which was 30 cm, as shown in Fig. 1. The steel beam was placed at the center of the model embankment in the width direction, and was purposely positioned close to the facing to investigate the influence of the flexible facing. The loading scheme is three dimensional, and can approximately represent periodic loading along the embankment axis, with an axial distance

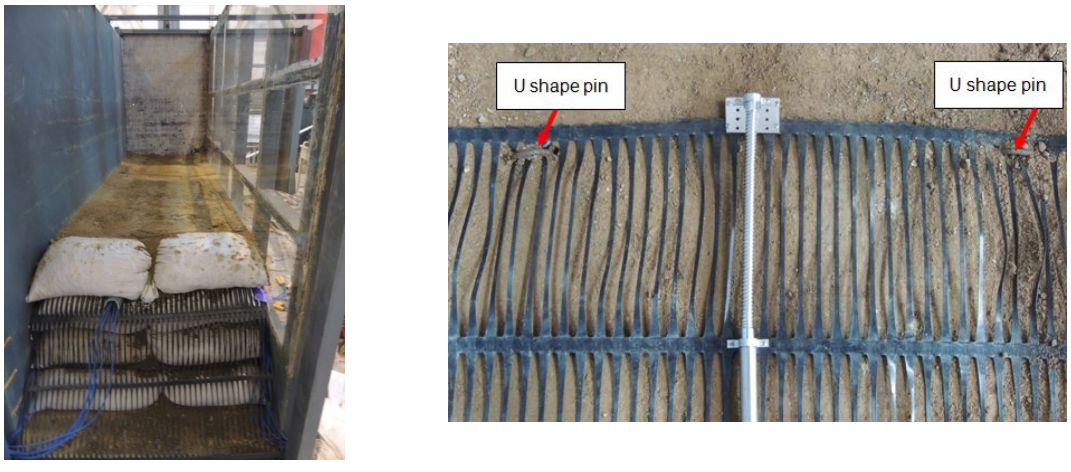


(a) (b)

Fig. 2 Arrangement of reinforcement layers: (a) Wrapped around facing; (b) U-shaped pins to anchor the reinforcement layers

of 1 m for the train. It is noted that the axial distance was smaller than actual applications (TB 10621 2009), and its influence on the embankment response will be discussed later.

The embankment was instrumented with static and dynamic earth pressure cells in both the horizontal and vertical directions, LVDTs on the steel beam, LVDTs in front of the facing, and accelerometers, as shown in Fig. 1(a). Here LX-1 represents the lateral LVDT, LX-2 represents the vertical LVDT, AX represents the accelerometer, HS-X represents the static earth pressure cell placed in the horizontal direction, VS-X represents the one in the vertical direction, HD-X represents the dynamic earth pressure placed in the horizontal direction, and VD-X respresents the one in the vertical direction. Steel angles were placed between soilbags to serve as the targets for the front LVDTs (The B series shown in Fig. 1(a)). The geogrids were also instrumented with flexible displacement transducers (Yang *et al*. 2009a, 2010) for reinforcement strains, but the results were not reliable, and they are not presented in Fig. 1(a).

The test procedure was as follows. After the construction was completed, the embankment was covered and left without disturbance for 10 days. Static loading test was then carried out, the purpose of which was to have a general idea about the embankment response, and to calibrate the dynamic loading levels in the subsequent dynamic tests. It is necessary to calibrate the dynamic loading levels from the static test, because traditional method (the 1:2 method) to estimate the additional pressure induced by surface loading cannot be applied here due to the stiff crushed-stone layer. Each level of static load was maintained for at least two hours until stabilized vertical settlement. After the static test, the backfill surface was re-surfed, and the embankment was left without disturbance for another three days due to equipment availability. The dynamic loading test then followed. Three dynamic load levels were applied, each load level having 400,000 sinusoidal cycles. Under each load level, four loading frequencies were employed: 4 Hz, 6 Hz, 8 Hz, and 10 Hz, each with 100,000 loading cycles. In the dynamic test, between every 100,000 cycles the loading was stopped for 15 minutes to collect instrumentation data. The dynamic loading was applied using a liquid-actuated dynamic loading system, which has a dynamic loading capacity up to 1000 kN. Different types of dynamic loading with various loading frequencies may be applied. The dynamic force was applied to the steel beam as a concentrated load, which was then transferred to the embankment surface as dynamic pressure (Fig. 1(a)).

## 3. Static test results

### *3.1 Earth pressures*

Fig. 3 shows the increases of vertical earth pressures under different levels of concentrated load. Fifteen centimeters (15 cm) below the crushed stone and approximately under the center of the loading beam, the increase of earth pressure was about 60 kPa when the surface load was increased to 47 kN. This concentrated load and the associated earth pressure below the layer of crushed stone were employed as the reference for the subsequent dynamic loading. From Fig. 3 it can be seen that the vertical earth pressure induced by the applied load decreased significantly with depth. Because the crushed stone layer was much stiffer than the backfill soil, and because the test was designed to be three dimensional, it is difficult to determine the areas of influence from the applied load. But the average contact pressure beneath the loading beam was approximately 2.6 times larger than the increase of earth pressure 30 cm below the beam. From Fig. 3, it can be seen that when the depth was increased by 1.2 m, the vertical earth pressure reduced from 60 kPa to less than 10 kPa. The significance reduction of additional earth pressure in the reinforced soil might

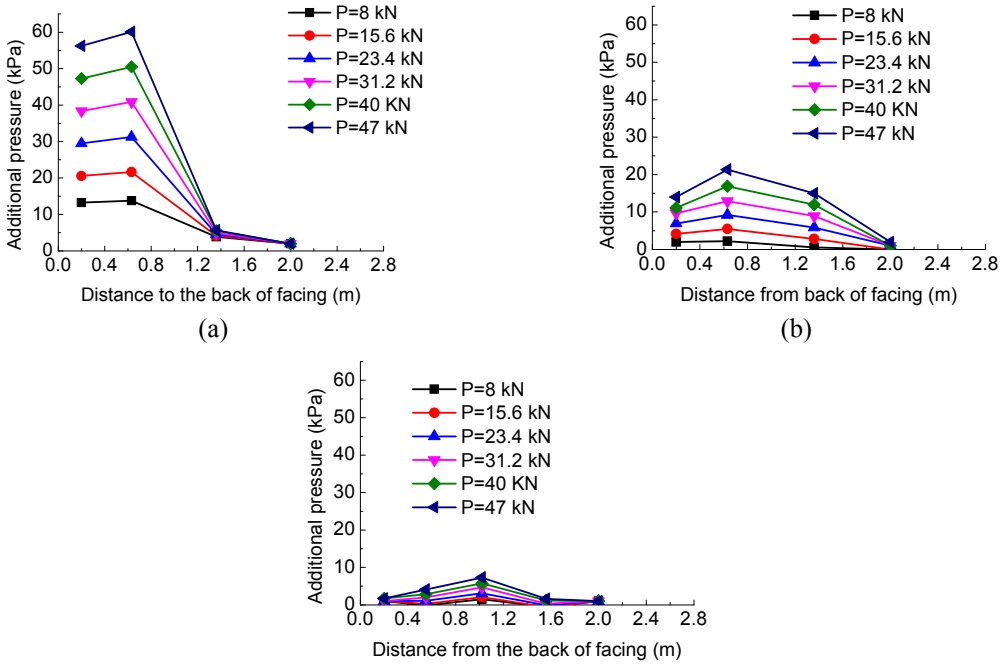


Fig. 3 Increase of vertical earth pressures during the static loading: (a) At $h$ = 1.35 m; (b) at $h$ = 0.75 m; (c) at $h$ = 0.15 m

have resulted from the function of reinforcement layers in spreading surface loading.

Fig. 4 shows the coefficients of lateral earth pressure at different heights and under different levels of concentrated load. A coefficient close to the active one was resulted at a height of 0.15 m under loading, and it slightly increased at the top ($h$ = 1.35 m) with an increase in the applied load. However, the coefficient at the mid height was much smaller. The active earth pressure herein was calculated using the simplified AASHTO equation with facing batter (AASHTO 2012). The increase of lateral earth pressure at the top was probably caused by the large deformation in the backfill soil, which resulted in strain softening, and the mobilized soil strength was smaller than the peak one. The small earth pressure at the mid height is believed to be the result of the

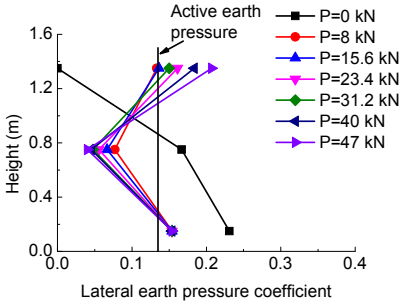


Fig. 4 Lateral earth pressure coefficients during the static loading

deflection of the flexible soilbag facing at that location. Similar small lateral earth pressures were also observed in wrapped-face or discrete panel walls under static loading (Tatsuoka 1993, Nakajima *et al*. 1996, Tajiri *et al*. 1996, Walters 2004). Lateral earth pressure at the base was close to the active one, which was induced by the base sliding of the soilbag facing. For reinforced soil walls with adequate toe constraint, the lateral earth pressure at the base is generally larger than the active one, as shown in many previous studies (Walters 2004, Yang *et al*. 2009a, Mirmoradi and Ehrlich 2015).

### *3.2 Vertical settlement*

Under the static loading, the backfill surface settled with an increase in the load level, but the rate of increase became smaller after the first stage of loading, as shown in Fig. 5. The flexible soilbag facing also settled with the backfill surface, but with a smaller magnitude. Close to the backfill surface, there existed a settlement difference of about 1 mm, indicating down-drag force on the facing column imposed by the reinforced soil. The average compression of the reinforced soil was small. The average compression strain was only slightly larger than 0.3% when the vertical earth pressure was 60 kPa.

### *3.3 Lateral facing displacement*

Fig. 6 shows the lateral facing displacements under static loading. One of the particular characteristics is the large displacement close to the base. It appears that the facing base slid under loading. The bottom soilbag layers were directly placed on the steel base of the test box, without

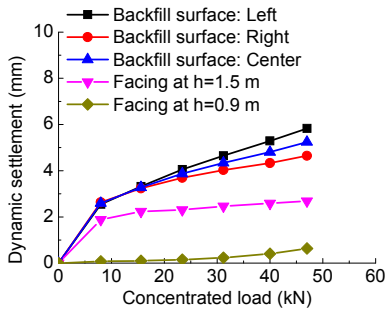


Fig. 5 Vertical settlements during the static loading

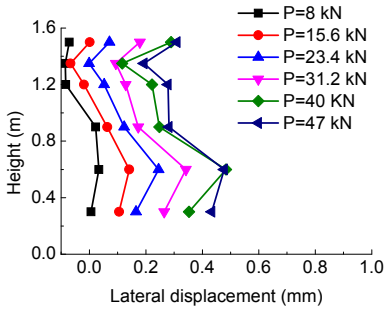


Fig. 6 Lateral facing displacements during the static loading

any restriction in the front. The friction between the soilbag and steel base was not large enough to provide the needed toe resistance. The sliding occurred at low loading level, and it continued to develop with an increase in the applied loading. Under a pressure of 60 kPa that occurred 15 cm below the crushed stone, the sliding was about 0.4 mm. The sliding also led to the slightly larger settlement close to the facing, as shown in Fig. 5. It is noted that similar sliding was also observed in wrapped-face reinforced soil walls with inadequate toe constraint (Bathurst *et al*. 2006, Benjamim *et al*. 2007). The larger settlement was the result of smaller confining pressure and looser state of the backfill soil close to the facing induced by facing sliding. Another particular characteristic is the larger deflection close to the mid height of the wall. The frictions between soilbags in this region might have been somewhat smaller, which was probably caused by inadequate compaction of the soilbags or improper soilbag alignment (Huang *et al*. 2008, Matsushima *et al*. 2008). This deflection has resulted in the smaller lateral earth pressure in Fig. 4.

## 4. Dynamic test results

After the static loading, the embankment was unloaded, and the backfill surface was re-surfed. Dynamic loading test was then carried out on the reinforced soil embankment, with three load levels: 32 kN – 62.4 kN, 47 kN – 80 kN, and 62.4 – 94 kN. Without dynamic effect, the corresponding mean pressures 30 cm below the loading beam, as inferred from the static test, were approximately 60 kPa, 80 kPa, and 100 kPa. These load levels were determined based on the Chinese standard (TB 10621 2009), which suggests an equivalent soil height of about 3 m for a design wheel load of 200 kN. It is also based on the measured soil stresses below the subgrades of some ballasted railways (Yang *et al*. 2009b, Bian *et al*. 2014). The load was applied in the manner of a sinusoidal curve, as illustrated in Fig. 7 for the low and mid loading levels at 4 Hz.

### *4.1 Vertical accelerations*

Large vertical accelerations were recorded below the crushed stone layer, as shown in Fig. 8. Under the same loading level, the vertical accelerations increased with an increase in the loading frequency. Particularly, there was a jump in the recorded accelerations when the loading frequency was 10 Hz. This result indicates that loading frequency may dominate the dynamic response of a reinforced soil wall under dynamic surface load (Payeur *et al*. 2015). In this case, the dynamic response increased with an increase in loading frequency, which is understandable. The theoretical

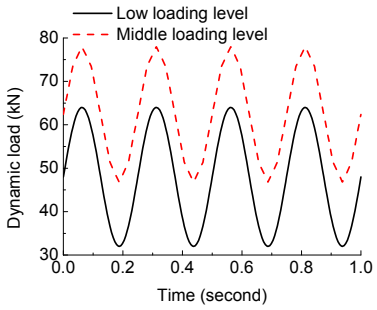


Fig. 7 Illustration of the dynamic loading

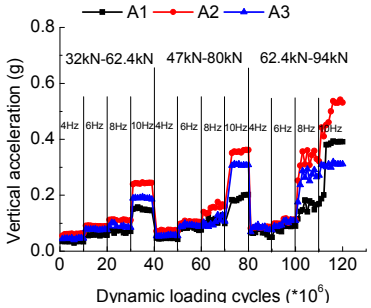


Fig. 8 Peak vertical accelerations during the dynamic loading

natural frequency of the embankment, neglecting the three-dimensional and nonlinearity effect, may be expressed as $f = v_p / 4H$, where H is the height of the embankment, and $v_p$ is the p-wave velocity. Although the wave velocity was not measured, it is expected to be higher than 150 m/s for the well-compacted gravelly soil in this study (Payeur *et al*. 2015). However, a jump of response at 10 Hz indicated that the resonant frequency may be close, but the theoretical natural frequency should have been much larger. The three-dimensional and nonlinear effect may have contributed to this difference. In the designs of such an embankment, it is therefore necessary to analyze its resonant frequency under train loads, but the three dimensional and nonlinear effect should be properly taken into account (Payeur *et al*. 2015).

### *4.2 Earth pressures*

Fig. 9 shows the variations of vertical dynamic earth pressures at two elevations with the increase of loading cycles. The first particular characteristic is the reduction of dynamic earth pressure at the top (Fig. 9(a)) when the exciting frequency was 10 Hz, which was caused by the possible resonance response discussed above. The earth pressure cell had a higher density than the backfill soil. When the surrounding soil was undergoing resonant vibration, the earth pressure cell might have been vibrating at a different frequency, and the phase lag might have led to the smaller dynamic earth pressure. This reduction was the result of measurement error, and cannot be interpreted as an actual decrease of earth pressure. The second characteristic that deserves attention is the large magnitude of dynamic earth pressure at the top. As pointed out above, the

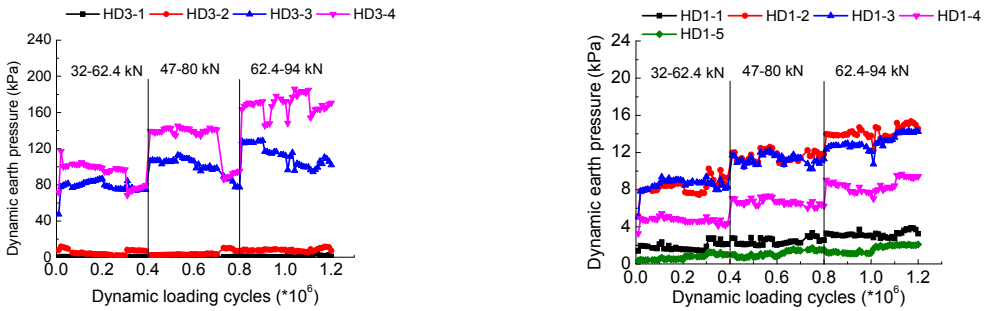


(a) (b)

Fig. 9 Dynamic peak vertical earth pressures: (a) At $h$ =1.35 m; (b) at $h$ = 0.45 m

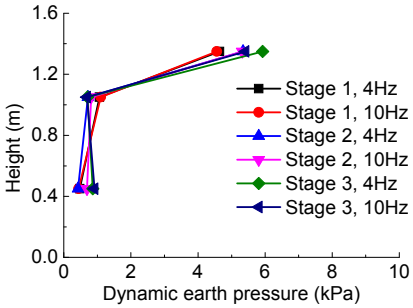


Fig. 10 Dynamic peak lateral earth pressures

mean applied pressure at the location without dynamic effect ranged from 60 kPa to 100 kPa, but the recorded values were in the range between 100 kPa and 180 kPa. The large difference signified the importance of dynamic effect, which seemed to increase with an increase in the applied load level. Proper consideration of this dynamic effect should be taken into account in the design and analysis of this type of structures. The last important characteristic is the reduction of dynamic earth pressure with depth. Approximately 1.2 m below the loading beam, the dynamic earth pressure reduced to a magnitude smaller than 20 kPa, and the attenuation coefficient of dynamic soil stress was as small as 0.11. This coefficient is much smaller than many measured values in ballasted or blastless railways with non-reinforced subbases or embankments (Bian *et al*. 2014). This further demonstrated the effect of reinforcement layers in distributing earth pressures.

Fig. 10 shows the dynamic lateral earth pressure close to the facing column. At the top and the bottom, the dynamic lateral earth pressures increased with an increase in the applied load levels, but the pressure decreased at the mid height, probably due to the facing deflection at the location. The maximum dynamic lateral earth pressure was only 18 kPa when the peak vertical earth pressure was 180 kPa. The small dynamic lateral earth pressure was probably the result of the lateral facing displacement that will be discussed in Section 4.4.

### *4.3 Vertical settlement*

The accumulative dynamic settlements were also not large, as shown in Fig. 11. The average dynamic compression strain after 1.2 million cycles of loading was approximately 0.3%. It should

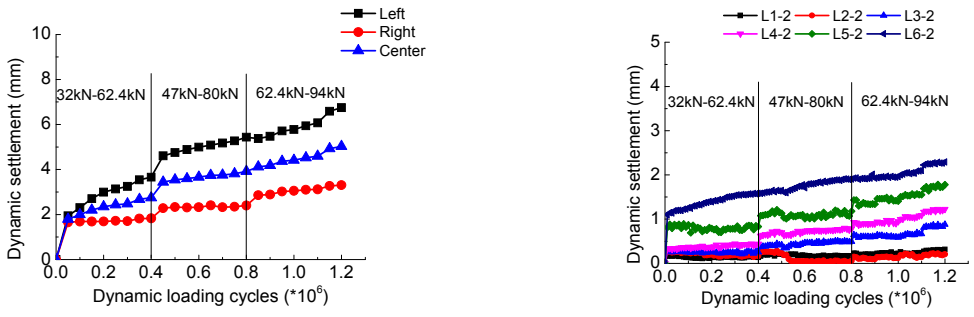


(a) (b)

Fig. 11 Dynamic peak vertical settlements: (a) Settlements of the loading beam; (b) settlements of the soilbag facing

be pointed out that the measured dynamic pressure below the layer of crushed stone ranged from 100 kPa to 180 kPa, depending on the mean dynamic loads. At the backfill surface, more than one third of the settlement occurred during the first 50,000 loading cycles in the first loading stage. The settlement then tended to stabilize with an increase in the loading cycle, but it increased again when the mean dynamic load increased. The influence of the loading frequency on the settlement was not significant. Fig. 11(b) shows the dynamic settlements of the soilbag facing at different elevations, which had a similar trend with the surface settlement, but the magnitude was smaller.

During the dynamic loading, the settlement was larger close to the facing, as shown in Fig. 11(a). One explanation is the accumulative lateral facing displacement (Fig. 12). The sliding of the facing column might have led to a smaller confining pressure and a looser state of the backfill soil close to the facing, making it more compressible under dynamic loading. Another possibility is the development of an internal failure surface in the reinforced soil. However, if such a surface actually developed, it must be in a very early stage, as the transparent sidewall did not reveal observable cracks or shear bands.

### *4.4 Lateral facing displacement*

As in the static loading case, the soilbag facing further slid on its base under dynamic loading (Fig. 12). Besides this sliding mechanism, the lateral deflection was larger at the top, which is understandable since the dynamic earth pressure was the largest at the location. There was also a larger deflection at the mid height, which was probably induced by the small shear strength between soilbags, as discussed in the static loading section. The maximum dynamic lateral displacement was about 0.5 mm (0.03% of the height).

### *4.5 Reinforcement strains*

Reinforcement strains were also instrumented in the test by means of flexible displacement transducers (Yang *et al*. 2009a, 2010). However, in this test, a transducer was bolted to the transverse ribs by two small steel frames, which resulted in a higher position than the plane of the geogid layer (Fig. 2(b)). Although the transducers were further protected by plastic covers, the subsequent soil compaction still led to their bending at some locations. As a result, some transducers gave strain readings at a magnitude of 0.5% to 1% right after soil compaction, and did not increase much with an increase of static and dynamic overburden soil stresses. The strains were therefore deemed to be unreliable, and the detailed results were not reported herein. However,

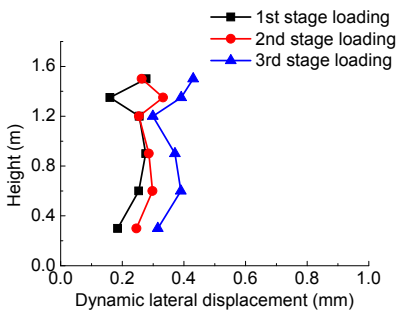


Fig. 12 Dynamic lateral displacements

the recorded strain readings were mostly smaller than 1%. Even if they represented the actual reinforcement elongations, they are still small considering the level of dynamic loading.

## 5. Discussions

The test box was 1 m wide, and the test was carried out to simulate the three dimensional and periodic loading conditions induced by a train with 1 m axial distance. This condition is different from actual application, which may have led to some boundary effects that affected the quantitative interpretations of the test results. However, the findings of this study may still be applied to actual applications. In addition, since very limited experimental studies exist that investigate the dynamic responses of reinforced soil embankments under simulated train loading, the test may provide the data to calibrate numerical procedures, which can then be employed to carried out in-depth studies for the quatitative behavior of reinforced soil railway embankments.

The model embankment was designed to have a flexible soilbag facing. Experimetal studies using other types of facings are undergoing in the authors' laboratory, and the collective results will provide the valuable information on the behavior of reinforced soil railway embankments, the contributions of facing stiffness and toe resistance (Tatsuoka 1993, Helwany *et al*. 1996, Huang *et al*. 2010, Leshchinsky and Vahedifard 2011, Ehrlich and Mimoradi 2013, Mirmoradi and Ehrlich 2015), and the influences of other structural parameters.

The large-scale test is an initial phase in a continuous study. It reveals some important aspects of GRS railway embankments under dynamic loading. However, the loading condition and the boundary conditions are different from those of actual GRS railway embankments, so the guidelines to design this type of earth structures under authentic railway loading cannot be developed at this stage.

## 6. Conclusions

A large-scale dynamic test on a reinforced soil railway embankment was carried out. The model embankment was 1.65 meter high and designed to have a soilbag facing. It was reinforced with HDPE geogrid layers at a vertical spacing of 0.3 m and a length of 2 m. The dynamic test followed a static loading test, with three levels of simulated wheel load. Altogether 1.2 million cycles of harmonic dynamic loading with four different exciting frequencies were applied to the embankment. The following conclusions can be obtained from the study.

(1) Geosynthetic reinforced soil with small reinforcement spacing, well-compacted backfill soil and high reinforcement stiffness had small compressibility under vertical dynamic loading, but proper toe restraint may be required for a reinforced soil embankment. Facing base sliding is possible under railway loading without sufficient toe resistant.
(2) Dynamic loading frequency might considerably influence the response of the reinforced soil embankment and deserves attention in the design.
(3) Dynamic effect led to much larger dynamic vertical earth pressures at the top of the embankment, but dynamic earth pressure decreased considerably with an increase of depth, possibly due to the load-spreading effect of reinforcement layers.

## Acknowledgments

The authors would like to thank the National Natural Science Foundation of China (Grant No. 51178280 and 51379082) for the support of this study.

## References

Abbasi, O., Ghanbari, A. and Hosseini, S.A.A. (2014), "An analytical method for calculating the natural frequency of reinforced retaining walls with soil-structure interaction effect", *Geosynth. Int.*, **21**(1), 53-61.

Abu-Hejleh, N., Zornberg, J.G., Wang, T. and Watcharamonthein, J. (2002), "Monitored displacements of unique geosynthetic-reinforced soil bridge abutments", *Geosynthet. Int.*, **9**(1), 71-95.

Adams, M.T., Nicks, J., Stabile, T., Wu, J.T.H., Schlatter, W. and Hartmann, J. (2011), "Geosynthetic reinforced soil integrated bridge system: Synthesis report", Rep. No. Federal Highway Administration (FHWA)-HRT-11-027; Washington, DC, USA.

Ansari, Y., Merifield, R., Yamamoto, H. and Sheng, D. (2011), "Numerical analysis of soilbags under compression and cyclic shear", *Comput. Geotech.*, **38**(5), 659-668.

Arab, R., Villard, P. and Gourc, J.P. (2001), "Use of reinforced soil bearing structures", *Ground Improv.*, **5**(4), 163-175.

ASTM D5030-04 (2004), Standard Test Method for Density of Soil and Rock in Place by the Water Replacement Method in a Test Pit; ASTM, West Conshohocken, PA, USA.

Bathurst, R.J., Vlachopoulos, N., Walters, D.L., Burgess, P.G. and Allen, T.M. (2006), "The influence of facing rigidity on the performance of two geosynthetic reinforced soil retaining wall", *Can. Geotech. J.*, **43**(12), 1225-1237.

Benjamim, C.V.S., Bueno, B.S. and Zornberg, J.G. (2007), "Field monitoring evaluation of geotextile-reinforced soil-retaining walls", *Geosynth. Int.*, **14**(2), 100-118.

Bhattacharjee, A. and Krishna, A.M. (2012), "Development of numerical model of wrap-faced walls subjected to seismic excitation", *Geosynth. Int.*, **19**(5), 354-369.

Bian, X., Jiang, H., Cheng, C., Chen, Y., Chen, R. and Jiang, J. (2014), "Full-scale model testing on a ballastless high-speed railway under simulated train moving loads", *Soil Dyn. Earthq. Eng.*, **66**, 368-384.

Cai, Z. and Bathurst, R.J. (1996), "Seismic response analysis of geosynthetic reinforced soil segmental retaining walls by finite element method", *Comput. Geotech.*, **17**(4), 523-546.

Ehrlich, M. and Mirmoradi, S.H. (2013), "Evaluation of the effects of facing stiffness and toe resistance on the behavior of GRS walls", *Geotext. Geomembr.*, **40**, 28-36.

El-Emam, M.M. and Bathurst, R.J. (2007), "Influence of reinforcement parameters on the seismic response of reduced-scale reinforced soil retaining walls", *Geotext. Geomembr.*, **25**(1), 33-49.

Fukubayashi, Y. and Kimura, M. (2014), "Improvement of rural access roads in developing countries with initiative for self-reliance of communities", *Soils Found.*, **54**(1), 23-35.

Guler, E. and Selek, O. (2014), "Reduced-scale shaking table tests on geosynthetic-reinforced soil walls with modular facing", *J. Geotech. Geoenviron. Eng.*, **140**(6), Article number: 04014015.

Hatami, K. and Bathurst, R.J. (2006), "Numerical model for reinforced soil segmental walls under surcharge loading", *J. Geotech. Geoenviron. Eng.*, **132**(6), 673-684.

Helwany, M.B., Tatsuoka, F., Tateyama, M. and Kojima, K. (1996), "Effects of facing rigidity on the performance of geosynthetic-reinforced soil retaining walls", *Soils Found.*, **36**(1), 27-38.

Huang, C.C., Matsushima, K., Mohri, Y. and Tatsuoka, F. (2008), "Analysis of sand slopes stabilized with facing of soil bags with extended reinforcement strips", *Geosynth. Int.*, **15**(4), 232-245.

Huang, B., Bathurst, R.J., Hatami, K. and Allen, T.M. (2010), "Influence of toe restraint on reinforced soil segmental walls", *Can. Geotech. J.*, **47**(8), 885-904.

Kachi, T., Kobayashi, M., Seki, M. and Koseki, J. (2013), "Reinforcement of railway ballasted track with geosynthetic bags for preventing derailment", *Geosynth. Int.*, **20**(5), 316-331.

Komak Panah, A., Yazdi, M. and Ghalandarzadeh, A. (2015), "Shaking table tests on soil retaining walls reinforced by polymeric strips", *Geotext. Geomembr.*, **43**(2), 148-161.
Koseki, J. (2012), "Use of geosynthetics to improve seismic performance of earth structures", *Geotext. Geomembr.*, **34**, 51-68.
Lee, K.Z.Z. and Chang, N.Y. (2012), "Predictive modeling on seismic performances of geosynthetic-reinforced soil walls", *Geotext. Geomembr.*, **35**, 25-40.
Leshchinsky, D. and Vahedifard, F. (2011), "Impact of toe resistance in reinforced masonry block walls: Design dilemma", *J. Geotech. Geoenviron. Eng.*, **138**(2), 236-240.
Ling, H.I., Leshchinsky, D., Mohri, Y. and Wang, J.P. (2012), "Earthquake response of reinforced segmental retaining walls backfilled with substantial percentage of fines", *J. Geotech. Geoenviron. Eng.*, **138**(8), 934-944.
Liu, H. (2009), "Analyzing the reinforcement loads of geosynthetic-reinforced soil walls subject to seismic loading during the service life", *J. Perform Constr. Facil.*, **23**(5), 292-302.
Liu, H. (2015), "Reinforcement load and compression of reinforced soil mass under surcharge loading," *J. Geotech. Geoenviron. Eng.*, **141**(6), Article No. 04015017.
Liu, H. and Ling, H.I. (2012), "Seismic responses of reinforced soil retaining walls and the strain softening of backfill soils", *Int. J. Geomech.*, **12**(4), 351-356.
Liu, H., Wang, X. and Song, E. (2011), "Reinforcement load and deformation mode of geosynthetic-reinforced soil walls subject to seismic loading during service life", *Geotext. Geomembr.*, **29**(1), 1-16.
Liu, H., Yang, G. and Ling, H.I. (2014a), "Seismic response of multi-tiered reinforced soil retaining walls", *Soil Dyn. Earthq. Eng*, **61-62**, 1-12.
Liu, S.H., Gao, J.J., Wang, Y.Q. and Weng, L.P. (2014b), "Experimental study on vibration reduction by using soilbags", *Geotext. Geomembr.*, **42**, 52-62.
Liu, S., Lu, Y., Weng, L. and Bai, F. (2015), "Field study of treatment for expansive soil/rock channel slope with soilbags", *Geotext. Geomembr.*, **43**(4), 283-292.
Lohani, T.N., Matsushima, K., Aqil, U., Mohri, Y. and Tatsuoka, F. (2006), "Evaluating the strength and deformation characteristics of a soil bag pile from full-scale laboratory tests", *Geosynth. Int.*, **13**(6), 246-264.
Lostumbo, J.M., Johnson, J. and Bernardi, M. (2014), "Back-to-back geosynthetic-reinforced MSE wall supporting elevated dual railway tracks", *Geotech. Special Publication*, **234**, 4167-4175.
Matsuoka, H. and Liu, S.H. (2003), "New earth reinforcement method by soilbags ('Donow')", *Soils Found.*, **43**(6), 173-188.
Matsushima, K., Aqil, U., Mohri, Y., and Tatsuoka, F. (2008), "Shear strength and deformation characteristics of geosynthetic soil bags stacked horizontal and inclined", *Geosynth. Int.*, **15**(2), 119-135.
Mirmoradi, S. and Ehrlich, M. (2015), "Numerical evaluation of the behavior of GRS walls with segmental block facing under working stress conditions." *J. Geotech. Geoenviron. Eng.*, **141**(3), Article number: 04014109.
Nakagawa, Y., Chen, G.L., Tatsui, T. and Chida, S. (2008), "Verification of vibration reduction characteristics with soilbag structure", *Proceedings of the 4th Asian Regional Conference on Geosynthetics*, Shanghai, China, June.
Nakajima, T., Toriumi, N., Shintani, H., Miyataka, H., and Dobahi, K. (1996), "Field performance of a geotextile reinforced soil wall with concrete facing blocks", In: (H. Ochiai, N. Yasufuku, K. Omine Eds.), *Earth Reinforcement*, Balkema, Rotterdam/Brookfield, pp. 427-432.
Payeur, J.B., Corfdir, A. and Bourgeois, E. (2015), "Dynamic behavior of a Mechanically Stabilized Earth wall under harmonic loading: Experimental characterization and 3D finite elements model", *Comput. Geotech.*, **65**, 199-211.
Srilatha, N., Madhavi Latha, G. and Puttappa, C.G. (2013), "Effect of frequency on seismic response of reinforced soil slopes in shaking table tests", *Geotext. Geomembr.*, **36**, 27-32.
Tajiri, N., Sasaki, H., Nishimura, J., Ochiai, Y. and Dobashi, K. (1996). "Full-scale failure experiments of geotextile-reinforced soil walls with different facings", In: (. Ochiai, N. Yasufuku, K. Omine Eds.), *Earth Reinforcement*. Balkema, Rotterdam, pp. 525-530.

Tatsuoka, F. (1993), "Roles of facing rigidity in soil reinforcing", *Earth Reinforcement Practice*, Balkema, Vol. 2, pp. 831-870.

Tatsuoka, F., Tateyama, M., Uchimura, T. and Koseki, J. (1997), "Geosynthetic-reinforced soil retaining walls as important permanent structures", *Geosynth. Int.*, **4**(2), 81-136.

TB 10621 (2009), Code for Design of High Speed Railway; Ministry of Railways of the People's Republic of China, Beijing, China. [In Chinese]

Uchimura, T. and Mizuhashi, M. (2005), "Effects of reinforcement stiffness on deformation of reinforced soil structures under small cyclic loading", *Proceedings of the 16th International Conference on Soil Mechanics and Geotechnical Engineering*: *Geotechnology in Harmony with the Global Environment*, Osaka, Japan, September.

Uchimura, T., Tateyama, M., Tanaka, I. and Tatsuoka, F. (2003), "Performance of a preloaded-prestressed geogrid-reinforced soil pier for a railway bridge", *Soils Found.*, **43**(6), 155-171.

Walters, D.L. (2004), "Behavior of reinforced soil retaining walls under uniform surcharge loading", Ph.D. Thesis; Queen's University, Ontario, Canada.

Wang, L., Zhang, G. and Zhang, J.M. (2012), "Centrifuge model tests of geotextile-reinforced soil embankments during an earthquake", *Geotext. Geomembr.*, **29**(3), 222-232.

Wang, L., Chen, G. and Chen, S. (2015), "Experimental study on seismic response of geogrid reinforced rigid retaining walls with saturated backfill sand", *Geotext. Geomembr.*, **43**(1), 35-45.

Wayne, M.H. and Miller, B. (1996), "Application of mechanically stabilized earth and segmental block walls", *Geotext. Geomembr.*, **14**(5-6), 277-287.

Wu, J.T.H., Lee, K.Z.Z. and Pham, T. (2006), "Allowable bearing pressures of bridge sills on GRS abutments with flexible facing", *J. Geotech. Geoenviron. Eng.*, **132**(7), 830-841.

Wu, J.T.H., Pham, T.Q. and Adams, M.T. (2013), "Composite behavior of geosynthetic reinforced soil mass", Rep. Federal Highway Administration (FHWA)-HRT-10-077; Washington, DC, USA.

Xie, Y. and Leshchinsky, B. (2015), "MSE walls as bridge abutments: Optimal reinforcement density", *Geotext. Geomembr.*, **43**(2), 128-138.

Xu, Y., Huang, J., Du, Y. and Sun, D. (2008), "Earth reinforcement using soilbags", *Geotext. Geomembr.*, **26**(3), 279-289.

Yang, G., Zhang, B., Lv, P. and Zhou, Q. (2009a), "Behaviour of geogrid reinforced soil retaining wall with concrete-rigid facing", *Geotext. Geomembr.*, **27**(5), 350-356.

Yang, L.A., Powrie, W. and Priest, J.A. (2009b), "Dynamic stress analysis of a ballasted railway track bed during train passage", *J. Geotech. Geoenviron. Eng.*, **135**(5), 680-689.

Yang, G., Ding, J., Zhou, Q. and Zhang, B. (2010), "Field behavior of a geogrid reinforced soil retaining wall with a wrap-around facing", *Geotech. Test. J.*, **33**(1), Paper ID GTJ102410.

Ye, B., Muramatsu, D., Ye, G.L. and Zhang, F. (2011), "Numerical assessment of vibration damping effect of soilbags", *Geosynth. Int.*, **18**(4), 159-168.

Zarnani, S., El-Emam, M.M., and Bathurst, R.J. (2011), "Comparison of numerical and analytical solutions for reinforced soil wall shaking table tests", *Geomech. Eng., Int. J.*, **3**(4), 291-321.

*GC*